Indoor Positioning via Artificial Magnetic Fields

Roman Kusche, Sven Ole Schmidt, and Horst Hellbrück

***Abstract*—Indoor positioning approaches are often based on electromagnetic wave signals with high frequency. However, signal reflections and the corresponding signal superpositions are challenging. As a result, there is still no indoor positioning technology established in commercial products, like smartphones or smartwatches. Recent publications have shown that this indoor positioning problem can be addressed by using artificial magnetic fields. However, the cubic attenuation of the magnetic field challenges technical implementations and limits the ranges. In this work, we propose an approach striving to address these issues of magnetic indoor positioning via a simple electro-mechanical single-anchor concept in combination with a small wearable sensor circuitry. The terrestrial magnetic field together with amplitude and phase measurements resolve the position and the orientation of the tag. The proposed indoor positioning approach via artificial magnetic fields is tested in a corridor for a spacial region of approximately $100\ \mathrm{m}^2$. The mean positioning error in this experiment was calculated to be $\mu = 1.0 \pm 0.81\ \mathrm{m}$. The proposed indoor positioning approach via artificial magnetic fields and the corresponding measurement system can therefore be useful alternatives when considering applications in which simple implementation is more important than positioning precision.**

***Index Terms*—Indoor positioning, magnetic fields, measurement system, single anchor system, wearable**

I. Introduction

POSITIONING of objects and persons has come to our daily life during the past decades. Especially, the usage of the GPS system for personal or vehicle navigation is included in many devices. However, this technology is designed for outdoor environments. There are many applications in which the object or person to localize is indoors or has at least no direct sight to GPS satellites, like navigation in airport buildings or shopping mall buildings [1], [2], [3]. Other applications for indoor positioning include health care systems, exemplary for patient tracking in hospitals [4]. Since GPS does not properly work in these cases, the focus was set on investigation of indoor localization technologies [5], [6], [7], [8], [9]. Fig. 1 shows five of these technologies which are frequently part of research articles.

Most indoor positioning approaches are based on the transmission and reception of electromagnetic high frequency signals [8]. Besides high availability of the electronic components, the behavior of electromagnetic waves them-self

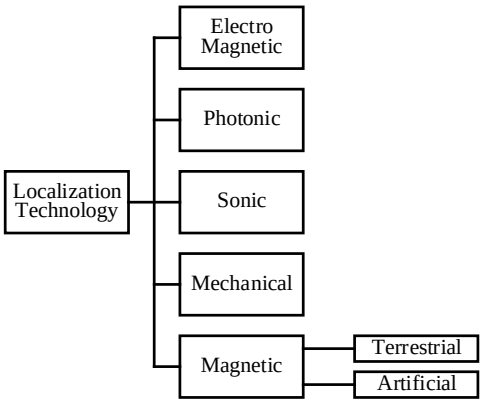

Fig. 1. Indoor localization technologies, based on [9].

are beneficial. The straight propagation characteristics and constant propagation speed allow to measure the distance between transmitter and receiver node from the Time-of-Flight (ToF) [9], [10]. If there are several transceivers at known positions inside the room, which are often called anchors, a receiver (tag) can calculate its own position by comparing the arrival times from the anchors, known as trilateration [7]. Alongside ToF, the current state of the art in radio technology enables the measurement of multiple transmission parameters. For example, signal strengths can be measured and used for triangulation and the radio signals can be modulated [7], [11], [12]. Despite these promising possibilities, this method has not yet been established. One of the main reasons is the multipath propagation caused by reflections of the transmit signal on physical surfaces [13]. At the receiver, the superposition of the received signal echoes is not distinguishable from only direct path components. Another approach for indoor localization is the usage of visible or non-visible light [14]. Here, the anchor nodes are modified lamps, transmitting modulated light into the room, while the receiving sensor of the tag can be a photo-diode or photo-transistor [15], [16], [17], [18]. By measuring different light intensities at receiver's side, distances to the anchors can be estimated and trilateration can be performed. A significant disadvantage of this technique is the influence of opaque material like cotton covering the sensor, which makes it not suitable for reliable systems with tags worn by persons. In addition, the signals depend on the sensor orientation. Sonic or ultra-sonic positioning setups are similar to electromagnetic high frequency techniques [19], [20]. On the one hand, they provide similar advantages. But on the other hand, the problems regarding multipath propagation and the resulting echo superposition at the receiver are very challenging. Mechanical localization techniques are less common as the ones previously described. In this case, the sensors

Manuscript received Month ??, 2021; revised Month ??, 2021; accepted Month ??, 2021. Date of publication Month ??, 2021; date of current version Month ??, 2021. This work was supported by the European Regional Development Fund under Grant LPW-E/1.2.1/765. *(Corresponding author: Roman Kusche.)*

Roman Kusche, Sven Ole Schmidt and Horst Hellbrück are with the Center of Excellence CoSA, Luebeck University of Applied Sciences, Luebeck 23562, Germany (e-mail:rk@romankusche.com; horst.hellbrueck@th-luebeck.de).

Horst Hellbrück is with the Institute of Telematics, University of Luebeck, Luebeck 23562, Germany.

gathering information regarding the tag position are physically interacting with the tag or the person to localize. Examples are force sensors on the floor and accelerometers or gyroscopes to detect transient position changes of the tag [21], [22]. In some applications, the mechanical localization technologies are used as additional information to improve the other principles [21], [23], [24].

In contrast to the approaches described before, magnetic fields are not reflected by mechanical surfaces and can only be affected by ferromagnetic materials [25]. Therefore it is a promising idea to use magnetic fields for indoor positioning. Magnetic field indoor positioning can be separated into two categories. The first uses the terrestrial magnetic field which is not perfectly homogeneous and influenced by the construction of the building and metal parts within it. Here, fingerprinting techniques are utilized for positioning, typically [26], [27], [28], [29]. However, whenever the field distribution changes, e.g. caused by the relocation of metal parts, reference measurements have to be performed. Moreover, the uniqueness of such measurement results cannot be predicted. The second category are artificial magnetic fields for localization. Especially the use of alternating fields is useful because they are distinguishable from the earth's magnetic field as well as from each other by frequency separation. This allows the simultaneous operation of several anchors. Systems published in the past, are based on strong electromagnets in combination with sensitive magnetic field sensors to detect the cubically decreasing field as far away as possible [30], [31], [32], [33], [34], [35], [36]. Other works use 2-dimensional electromagnet arrays for high resolutions [37]. Similar to other indoor position techniques, the received strengths of the signals sent from anchors are evaluated to estimate the distance between the nodes and to localize the tag via trilateral algorithms. High currents of several Amperes to generate suitable magnetic field strengths are technically challenging. On the one hand, it is difficult to control or modulate such high currents. On the other hand, the coils used in some works have too large dimensions for being widely used in indoor positioning applications [30], [31], [34]. Sheinker et al. for example, published a manuscript in which the magnetic field is generated by a coil with a dimension of $0.5\ m$ by $0.5\ m$ and a power consumption of $160\ W$ striving to use commercially available smartphones or tablets as tags [34]. Blankenbach et al. published a similar setup in which the diameter of the transmitting coil was $50\ cm$, electrically driven by a current of $12\ A$ [31]. In combination with a sensing tag realized via magnetoresistive transducers, ranges of up to $16.6\ m$ were achieved. The system proposed by Abrudan et al. can decrease the power consumption of such a setup to $1.2\ W$ and demonstrated a range of $10\ m$ within a building, but uses a cubic magnetic transmitter ($30\ cm$ x $30\ cm$ x $30\ cm$) and portable receiving coils [36].

However, there are also works showing up a trade-off between geometrical dimensions, technical complexity, power consumption and range, demonstrating the applicability of these electromagnetic approaches in realistic indoor environments. In a recent work, Sheinker et al. reduced the size of the electromagnets to $15\ cm$ x $15\ cm$ and kept the power consumption in a reasonable range of $3.6\ W$, while covering a localization area of $7\ m$ x $7\ m$ [35]. Even more compact transmitting coils with a diameter of $14\ cm$ were used in the approach, published by Pasku et al. [33]. By combining seven of these transmitters with a power dissipation of just $150\ mW$ each, an indoor area of $15\ m$ x $12\ m$ was covered. With a mean positioning error below $0.5\ m$ and a standard deviation $\leq 11\ cm$, this work has demonstrated its usability for the intended application of indoor navigation.

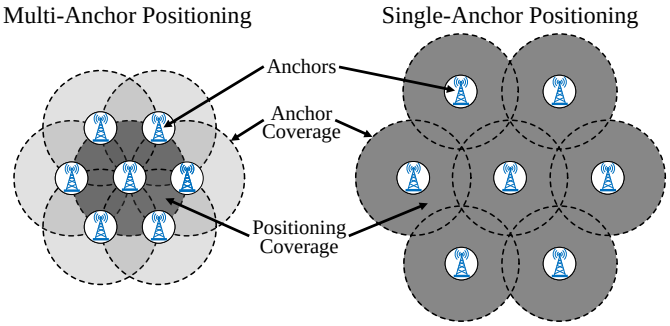

Fig. 2. Theoretical Approach for multi-anchor and single-anchor positioning techniques.

In some applications, such as navigation in a shopping mall, this high precision is not necessary. Therefore, the motivation of this work is to further reduce the technical instrumentation effort while accepting lower positioning precision.

For that, our approach strives to keep the number of anchors small by avoiding multi-anchor positioning, which is needed for trilateral signal analysis. In Fig. 2 this conventional approach is compared to a single-anchor positioning setup. It can be seen that the need of receiving the signal from only one anchor allows to increase the distance between the anchors. Thus, the same number of anchors can cover a significantly larger area.

In addition to decreasing the number of anchors, their technical implementation will be simplified and costs are kept low by the development of an electro-mechanical solution.

II. Materials and Methods

This section provides the theoretical background of the rotating magnetic field, the measurement parameters, our positioning approach and the implementation details.

A. Rotating Magnetic Field

Since the approach in this work is based on an artificial alternating magnetic field, its characteristics will be described briefly. For that, the geometrical distribution of the flux density for a cylindrical permanent magnet was simulated two-dimensionally [38], [39]. The magnet with a length of $l = 100\ \mathrm{mm}$, a diameter of $D = 10\ \mathrm{mm}$ and a remanence of $B_\mathrm{r} \approx 13.5\ \mathrm{mT}$ is located in the center of Fig. 3 with the north pole oriented in y-direction. Assuming a distance of 2 m, at position Pos. 1, the field strength in the y-direction is maximum and the x-component of the field strength at this position is 0. At Pos. 2 the conditions are different. The y-component reaches its maximum at this point and the x-component is 0. It should be noted that the magnetic

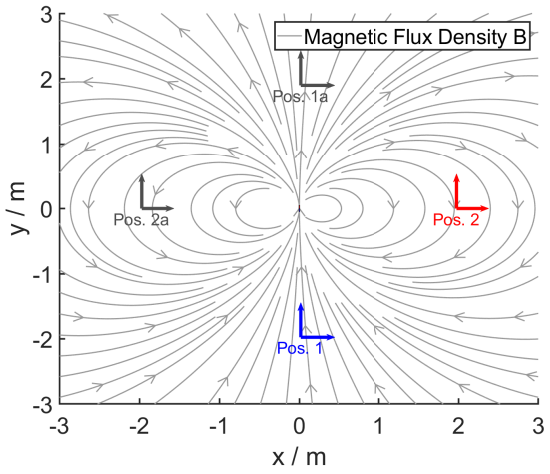

Fig. 3. Two-dimensional simulation of the field distribution of a permanent magnet.

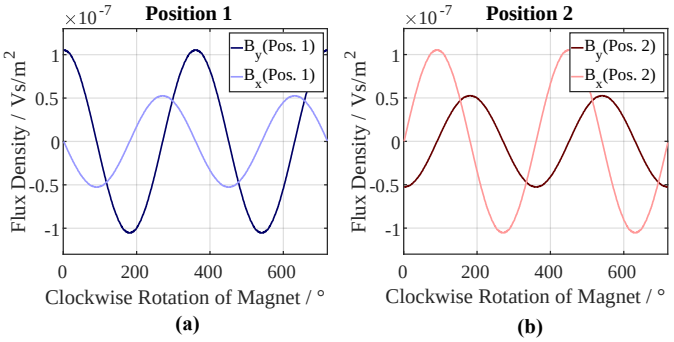

Fig. 4. Transient changes of the magnetic x- and y-field components during clockwise rotation of the permanent magnet in Fig. 3.

field is symmetrical, so the resulting magnetic field vector at positions Pos. 1 and Pos. 1a respectively Pos. 2 and Pos. 2a is identical.

If the magnet, whose dimensions are much smaller than its distance to the sensor, is rotated, harmonic oscillations occur for the x- and y-components of the field strength. This is shown in the simulation results in Fig. 4. The amplitudes of the components resulting from the rotation of the magnet end up in a ratio of 2:1 and 1:2 respectively. The corresponding direction dependent, elliptical field strength is shown in Fig. 5.

B. Positioning Approach

Next, we present the underlying indoor positioning method of this work, based on previously published single-anchor setups [40]. The previously described ambiguity of the magnetic field information is neglected at this point for simplification. The position of the target person wearing the tag sensor node is determined from a combination of sensor data and a synchronization signal.

In Fig. 6 the principle of the approach is illustrated. It consists of an anchor and a tag. The anchor consists of a rotating magnet, whose current north pole orientation φ_{Tx} in relation to the Earth's north pole is known and transmitted to the tag, worn by a target person.

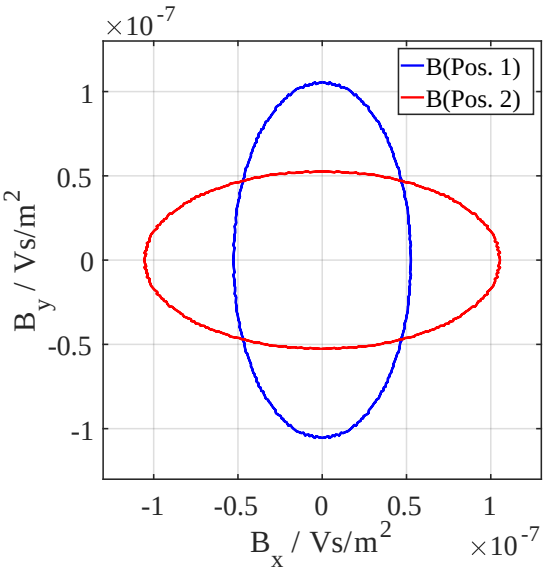

Fig. 5. Direction dependent signal amplitudes at Pos. 1 and Pos. 2, resulting in ellipses with the ratio 1:2.

The distance d between tag and anchor and the position on the corresponding dashed radius are unknown and shall be determined. To localize the target, the tag measures two parameters. The Earth's magnetic field is determined to ascertain the sensor orientation $\varphi_{\mathrm{Orient.}}$. Additionally, the artificially generated alternating magnetic field strength and its phase shift φ_{Rx} versus the received reference signal are measured. Since the Earth's magnetic field does not change over time and the generated field contains only alternating components, the signals can easily be separated by filters. However, the values of the terrestrial field depend on many factors such as the shielding characteristics of the building and cannot be predicted. Therefore, a-priory knowledge regarding the field strengths in every specific room is required, which can be acquired in advance of actual measurements.

Assuming that the magnetic field strength decreases cubically with distance and knowing the physical properties of the rotating magnet, the distance d can be determined by the amplitude of the signal. Using the equation (1) the phase angle $\varphi_{\mathrm{Pos.}}$ can be calculated, which defines the position on the dashed radius.

$$\varphi_{\mathrm{Pos.}} = \varphi_{\mathrm{Rx}} + \varphi_{\mathrm{Tx}} - \varphi_{\mathrm{Orient.}} \tag{1}$$

C. Technical Implementation

In order to test the technical feasibility of the proposed method and to carry out first test measurements, a measurement system is realized. In this section development of the anchor, the tag and finally the signal processing will be described.

As mentioned, the property of the high field strengths of neodymium magnets is used and the alternating field is generated only by its rotation. For this purpose an anchor as shown in Fig. 7 was realized. It consists of a wooden construction with a height of $h = 1$ m to which a DC motor is

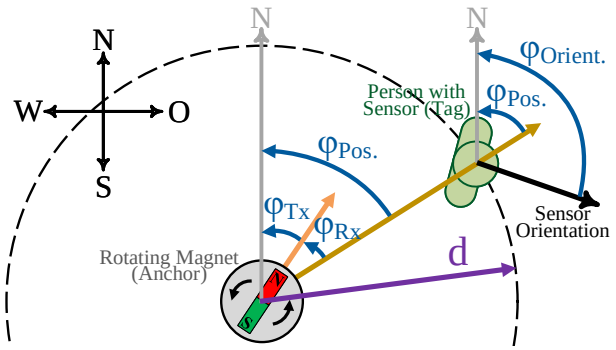

Fig. 6. Principle of the indoor positioning approach using artificial alternating magnetic fields.

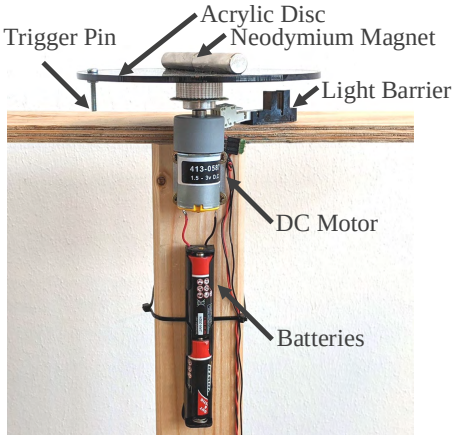

Fig. 7. Setup of the anchor that generates the alternating magnetic field via rotating a permanent magnet. The cylindrical magnet ($l = 100$ mm, $D = 10$ mm) is placed on a circular acrylic disc, driven by a motor.

attached that rotates a circular acrylic disc ($D_{\mathrm{Disc}} = 130$ mm). In order to keep the mechanical risk potential of the initial setup low but still use a frequency range above typically required positioning update rates, the rotational speed of the motor was chosen to be $\approx 10\ Hz$. The motor is powered with 3 V_{DC} via two AA batteries and its power consumption was measured to be $P_{\mathrm{anchor}} \approx 750$ mW. On the center of the disc a cylindrical neodymium magnet with the same characteristics ($l = 100$ mm, $D = 10$ mm, $B_{\mathrm{r}} \approx 13.5$ mT $\pm$ 0.3 mT) as used in the simulation above is positioned. For synchronization purpose, a trigger pin is attached to the bottom of the disc, which passes a light barrier with each rotation. This timing information is sent to the tag in order to enable a reconstruction of the current magnet angle.

For the tag, a similar wooden construction is used on which a magnetic sensor board is mounted. This printed circuit board (PCB) contains a magnetic field sensor (AFF755B from Sensitec) based on the anisotropic magnetoresistive effect (AMR), analog components for signal processing, and power supply circuitry. A photograph of the PCB is illustrated in Fig. 8. Its dimensions are 46×29 mm^2.

The principle of signal processing is shown in Fig. 9. It is composed of an anchor, a tag and a common external analog-to-digital converter (ADC, ADS131E06 from Texas Instruments). From the anchor, only a trigger signal of the

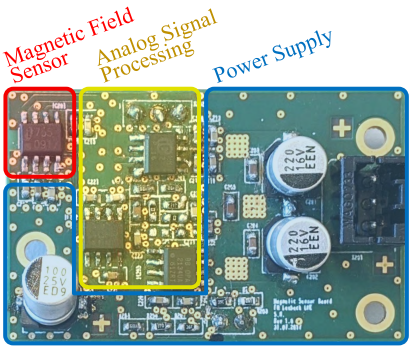

Fig. 8. Magnetic sensor board, including the field sensor, analog signal processing components and power supply circuitry.

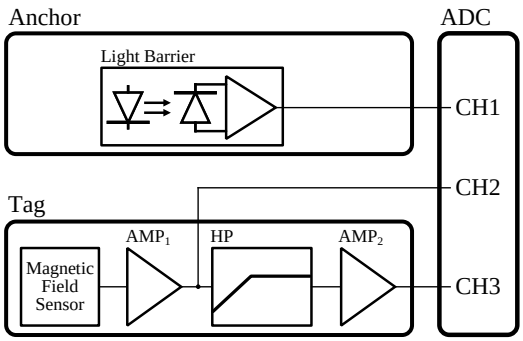

Fig. 9. Block diagram of the measurement circuitry and analog signal processing.

light barrier is acquired by channel CH1 for synchronization of anchor and tag. Under real measurement conditions, the ADC would be part of the tag and the trigger signal from the anchor would be transmitted via a wireless communication channel to the tag. However, for this experimental setup, the trigger signal is transmitted via a wire to the common ADC.

The processing chain of the tag starts by amplifying the analog voltage signal from the magnetic field sensor. An instrumentation amplifier (AMP_1, INA129 from Texas Instruments) amplifies the sensor signal with a gain of $\mathrm{G} = 100$. Its output is directly connected to channel CH2 of the ADC to digitize the raw data including both the constant (DC) and the alternating (AC) components of the magnetic field. In contrast to the constant Earth's magnetic field, the alternating artificial field decreases cubically over distance to the anchor. For obtaining high distance ranges, it is therefore useful to amplify the AC component of the measured signal, additionally. To avoid clipping, caused by the strong DC components, the signal is high-pass filtered (HP, N=1, $\mathrm{f_c} = 0.1$ Hz) before. Then the filtered signal is amplified by two operational amplifier stages (AMP_2, OPA2134 from Texas Instruments) with a total gain of $\mathrm{G} = 120$. Finally, the ADC converts the signal at Channel CH3.

All three channels are converted with a sampling rate of $\mathrm{f_s} = 1000$ SPS and a resolution of 24 Bits. For further signal processing, the digitized data is transmitted via an existing acquisition system to a PC [41], [42].

The required compass information to determine $\varphi_{\mathrm{Orient.}}$ can easily be extracted from the signal acquired via ADC channel

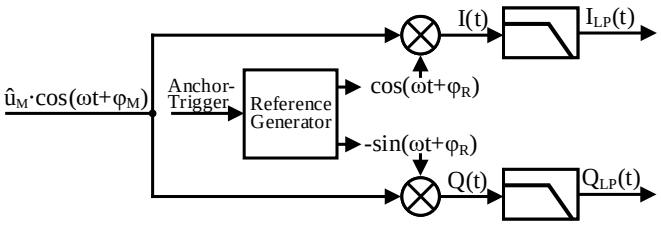

Fig. 10. Principle of the dynamic IQ-Demodulation for calculating the amplitude and phase shift of the digitized sensor signal.

CH2. However, to measure the amplitude and phase of the AC signal component, a more complex signal processing is necessary. This is especially the case if a constant motor speed cannot be ensured. For that, we implemented a dynamic IQ-demodulation. As illustrated in Fig. 10, the measured signal with the unknown amplitude $\hat{u}_M$ and phase φ_M is multiplied by two normalized orthogonal harmonic signals with the reference phase φ_R and the same frequency ω. To generate these reference signals, the measured trigger signal from the anchor is used. After the multiplications, both the signals are filtered by zero-phase low-pass filters (N=1, $f_c = 0.2$ Hz).

With the resulting signals $I_{LP}(t)$ and $Q_{LP}(t)$ the magnitude and phase values can be calculated according to equations 2 and 4.

$$\hat{u}_M = 2\sqrt{I_{LP}^2 + Q_{LP}^2} \tag{2}$$

$$\varphi_M = \arctan \frac{Q_{LP}}{I_{LP}} \tag{3}$$

Considering the anchor trigger to be in phase with the rotating magnet, φ_R corresponds to φ_{Tx} and φ_M corresponds to φ_{Rx}. Since in the proposed setup shown in Fig. 7 there is an angle between the trigger pin and the neodymium magnet of $\varphi_{Trigger}$, a correction is performed according to

$$\varphi_{Rx} = \varphi_M - \varphi_{Trigger} \tag{4}$$

.

III. Results and Discussion

A. Characterization

Before performing actual measurements for indoor positioning, the realized setup is characterized. To analyze the decrease of the signal amplitude over distance and directional dependencies, the measurement setup depicted in Fig. 11 was used. As shown, the anchor with the rotating magnet was placed at a fixed position and the tag with the sensor board was moved to several different positions. The distance D between magnet and sensor was changed in 50 cm steps. In each of these positions, the rotation angle α was changed in 22.5° steps every 30 s until a 360° rotation was completed.

The acquired raw data from ADC channel CH2 for $D = 1.5$ m is shown in Fig. 12. The changes in the signal offset every 30 s are caused by the mentioned rotating of the sensor and the corresponding change of the terrestrial field strength. During this measurement, the amplified output voltage from the instrumentation amplifier varies between

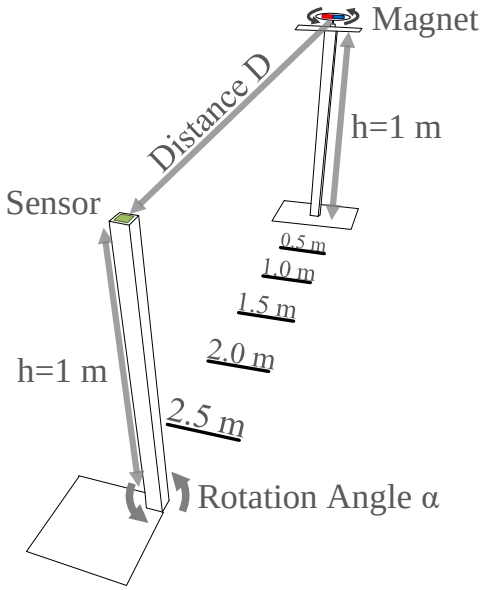

Fig. 11. Measurement setup to characterize the realized approach.

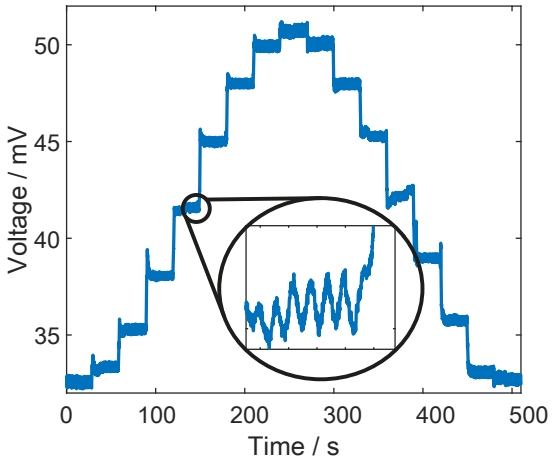

Fig. 12. Raw data of the characterization measurement at $D = 1.5$ m, digitized with ADC channel CH2. The signal is a superposition of the terrestrial magnetic field (DC) and the artificial magnetic field.

32 mV and 51 mV. For the positioning measurements in the next section, the DC components were averaged over 10 s each and compared with a real compass. This relationship between measured DC voltage and actual orientation has been stored to a look-up table in the MATLAB file format. To increase the resolution to 1°, a linear interpolation of the table was performed, enabling the determination of the tags orientation compared the terrestrial magnetic field.

Since the AC signal component is super-positioned by noise and other disturbances, the dynamic IQ demodulation explained above is used. For that, the amplified and filtered data from CH3 is used, yielding higher voltage values in the polar plot in Fig. 13. In this plot, it can be seen, that there is a significant signal decrease when changing the distance between magnet and sensor, which was expected due to the cubical behavior of the magnetic field in free space. Furthermore, the field strength measured in y-direction (0°) is

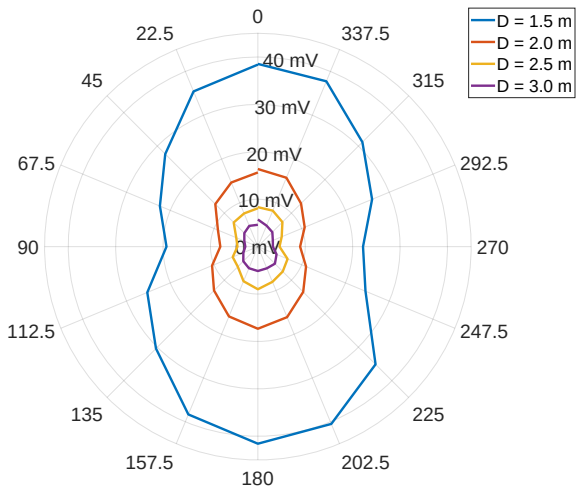

Fig. 13. Measured AC signal amplitude depending on distance and sensor orientation.

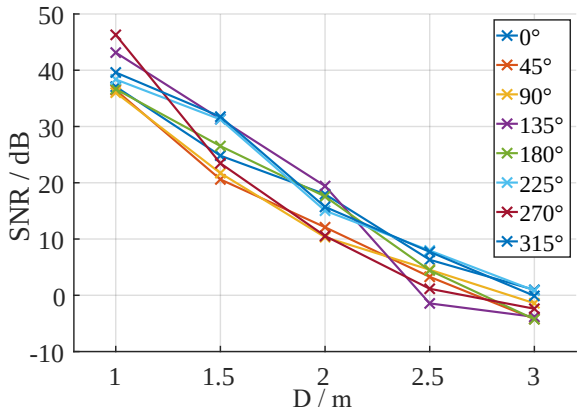

Fig. 14. Signal-to-Noise ratio of the digitized sensor signal depending on distance and sensor rotation.

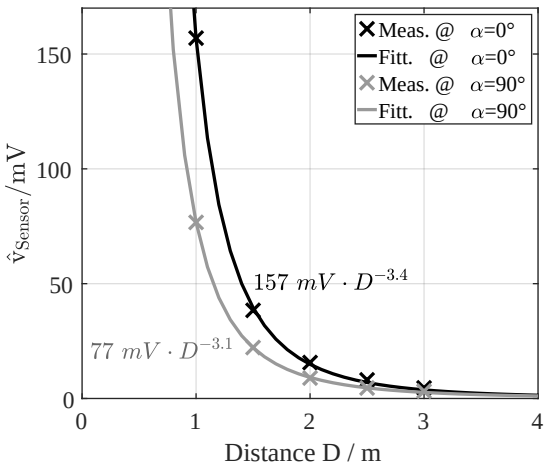

Fig. 15. Approximation of the sensor characteristics. The measurement results for $\alpha = 0°$ and $\alpha = 90°$ are fitted to power functions.

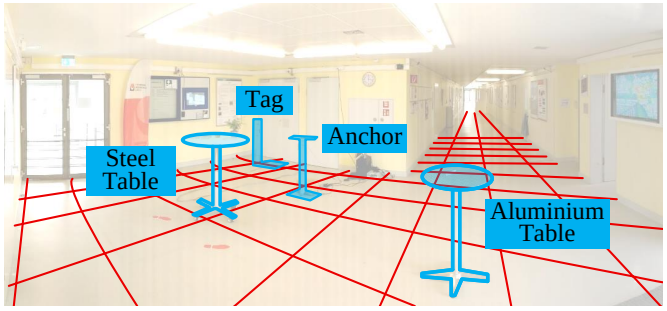

Fig. 16. Setup for measurements under realistic conditions in a corridor. While the anchor position remained constant, the tag was moved on the red grid. The metallic tables are used for the investigation of signal influences.

approximately twice as high as that measured in the x-direction (90°/270°), corresponding to the elliptical characteristic of the field.

The strong decrease of the field strength when moving the sensor away from the rotating magnet affects the signal-to-noise ratio (SNR) of the measured signal. In Fig. 14 the corresponding values are plotted over D. It can be seen that the SNR for small distances is better than 36 dB but decreases below 0 dB at $D = 3$ m.

The acquired measurement data is a basis to model the actual sensor amplitude over distance via a fitting function. Therefore, the maximum and the minimum of amplitudes at $\alpha = 0°$ and $\alpha = 90°$ are analyzed separately. The approximated amplitude functions are plotted in Fig. 15 As expected, the linear factor at $\alpha = 0°$ (157 mV) is about twice as high as that of the measurement at $\alpha = 90°$ (77 mV). Due to the cubic behavior, exponents of 3 would be expected. However, the magnetic field as a function of D decreases more than expected. The actual measured exponents are 3.4 and 3.1, respectively. The reason could be the influence of the reinforced concrete ceiling, floor and walls. It must be noted that these determined values are only valid of the specific measurement setup.

B. Measurement in Realistic Environment

After characterizing the measurement approach under ideal conditions, a more realistic localization setup was realized in a corridor of an office building, as shown in the photograph in Fig. 16. The maximum width of this corridor is 7.7 m and the maximum length is more than 40 m, whereat only 12 m are considered in this experiment. The exact dimensions can be taken from the following illustrations. In this experiment, the anchor position remained constant and only the tag position was changed according to the red drawn grid with distances of 1 m each. Only translational motions were performed, whereat the sensor was permanently orientated in x-direction. For not exclusively analyzing the effects of the reinforced concrete walls and steel door frame, two metallic tables were placed in the room, additionally. One is made of aluminum, the second is mostly made of steel.

After switching on the anchor, the magnetic fields were measured along the grid for durations of 10 s each. The digitized data were processed with the proposed IQ demodulation and averaged afterwards. Fig. 17 plots the measured magnitude values, whereas the cubic voltage decrease was compensated for better visualization. It has to be noted that the value at the position ($x \approx 5$ m, $y \approx 5$ m) is only an approximation because

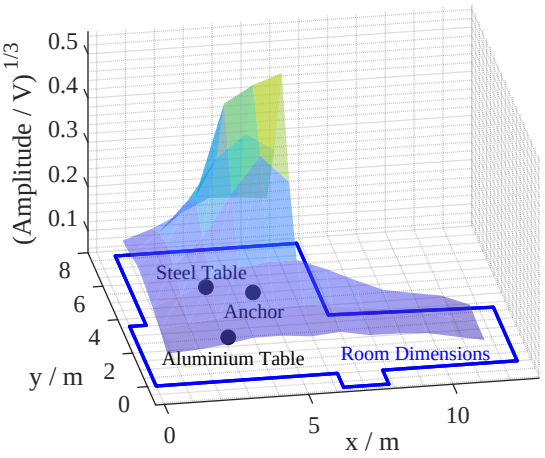

Fig. 17. Measured magnitude values of the artificial magnetic field components. For better visualization the cubic voltage decrease was compensated as noted in the axis label. The resulting values vary from 0.062 to 0.54.

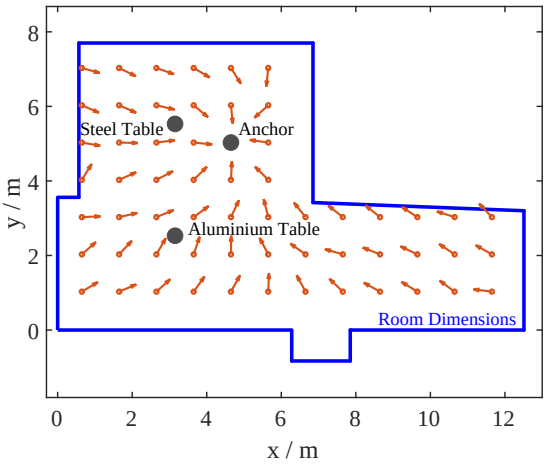

Fig. 18. Measured phase values, plotted as normalized vectors.

of the anchor position there. The resulting plot decreases as expected over the distance to the anchor. This behavior occurs over the whole spatial measurement region. However, this decrease is not linear in this plot, indicating that the raw data decreases not exactly cubically. Also in this measurement, we could not find any significant influences by the metallic tables on the characteristics of the results.

The corresponding phase values were calculated under consideration of the terrestrial magnetic field, as described in section II-B. The corresponding normalized vectors are plotted for each grid position in Fig. 18. As described in Sec. II, the proposed approach has a phase ambiguity of $\pm 180°$. For this reason, some vectors had been inverted to present the expected plot. Under realistic measurement conditions further information is necessary to eliminate this ambiguity. This can be generated via motion tracking algorithms or sensor fusions. Almost all arrows point in the direction of the anchor. However, at some positions which are affected by close walls or shading effects, the directions of the vectors are falsified. In addition, deflection effects occur, seeming to have a systematic behavior caused by the combination of the field characteristics and the sensor. It is conceivable that applying specific models for metal-rich indoor environments could decrease the impact of the walls or the metal tables in the room [43].

C. Positioning via Measured Signals

The actual goal of the proposed measurements is indoor positioning. To test the approach's suitability for realistic applications, the measured data is used to calculate the tag positions. Although the phase information can be used directly for this purpose, the measured amplitude values must still be assigned to the corresponding distances to the anchor. Measurements in Sec. III-A show that the amplitudes also depend on the sensor orientation. However, since the distance has a much stronger effect on the measured values, the elliptical characteristic is neglected for this calculation. Instead, results from Fig. 15 are averaged to the generalized transfer function 5.

$$D = \left(\frac{\hat{v}_{\text{Sensor}}}{117\ \text{mV}} \right)^{-\frac{1}{3.25}} \ \text{m} \tag{5}$$

Fig. 19 marks the resulting calculated positions as crosses and the actual measurement positions as circles. The color labeling simplifies the assignment of the measuring points. The accuracy of the localization increases by decreasing distance between the fixed anchor and the tag. For large distances between the nodes, the accuracy of the localization decreases the more difficult it becomes to assign the measured positions to the actual ones. It can also be seen that the measured positions have a curved characteristic, which can be explained by the behavior of the phase results, described before. The mean positioning error in this experiment and its standard deviation were calculated to be $\mu = 1.0 \pm 0.81$ m. Based on the specific characteristic of these miss-allocations between measurement and the actual measurement position, it is assumed that more suitable position reconstruction approaches can significantly improve these results.

It must be taken into account that changes of the specific measurement conditions such as rearranging furniture can influence the AC as well as the DC components of the magnetic field. Furthermore, the exact physical characteristics of the permanent magnet must either be known or measured prior to the actual localisation procedure.

IV. Conclusion

The results of this work have endorsed that magnetic indoor positioning is an approach that is technically feasible and useful. In contrast to other publications, the anchor used in this work is based on a very simple electromechanical setup. Its dimensions as well as power consumption are comparable to the results of previous works, which are based on electromagnetic approaches. Compared to conventional triangulation or trilateration approaches, the setup proposed in this work requires less anchors. However, the proposed single-anchor positioning method has the disadvantage that the phase measurement has an uncertainty of $\pm 180°$, which must be considered in the deployment. Additional information like

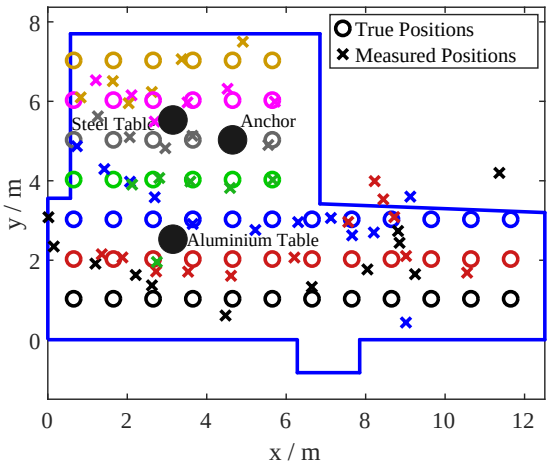

Fig. 19. Actual measurement positions (circles) and via the measurement results calculated positions (crosses) of the tag in the corridor.

motion tracking algorithms or sensor fusions can solve this uncertainty in the future.

In contrast to an expected cubic attenuation of the magnetic field, the measurement results from our setup indicated an exponent between 3.1...3.4, calling for calibrations. In the future, further measurements under different conditions are necessary to decide if area specific a-priory information is required. Since it is obvious that the accuracy of compass calibration affects the positioning precision, these measurements would also be useful to investigate the actual need for compass calibrations in every new measurement area. Apart from these challenges, we have shown that localizing in a realistic environment was successful. The resulting measurement errors depend on the measurement position and are higher than those of other works but are acceptable for several applications like indoor navigation in shopping malls or hospitals.

Caused by the cubic decrease of the magnetic field strength due to the distance, the spacial range of the demonstrated magnetic indoor positioning is limited. The higher the distance between anchor and tag, the higher the the signal-to-noise ratio, leading to the large measurement errors at the outer regions of the investigated room. In the future we increase the sensitivity of the sensor setup and the generated magnetic field strength. Also a more complex positioning algorithm will decrease the error of position estimation and probably increase the achieved spacial ranges.

ACKNOWLEDGMENTS

The work presented here is the result of a research project of the Center of Excellence CoSA, which is funded by the state of Schleswig-Holstein, Germany (project number: LPW-E/1.2.1/765). Horst Hellbrück is adjunct professor at the Institute of Telematics of University of Lübeck.

REFERENCES

[1] J. Guerreiro, D. Ahmetovic, D. Sato, K. Kitani, and C. Asakawa, "Airport accessibility and navigation assistance for people with visual impairments," in *Proceedings of the 2019 CHI Conference on Human Factors in Computing Systems - CHI 19*. ACM Press, 2019.

[2] H. J. Jang, J. M. Shin, and L. Choi, "Geomagnetic field based indoor localization using recurrent neural networks," in *GLOBECOM 2017 - 2017 IEEE Global Communications Conference*. IEEE, dec 2017.

[3] A. Puikkonen, A.-H. Sarjanoja, M. Haveri, J. Huhtala, and J. Häkkilä, "Towards designing better maps for indoor navigation," in *Proceedings of the 8th International Conference on Mobile and Ubiquitous Multimedia - MUM 09*. ACM Press, 2009.

[4] J. Yang, Z. Wang, and X. Zhang, "An iBeacon-based indoor positioning systems for hospitals," *International Journal of Smart Home*, vol. 9, no. 7, pp. 161–168, jul 2015.

[5] G. Dedes and A. Dempster, "Indoor GPS positioning - challenges and opportunities," in *VTC-2005-Fall. 2005 IEEE 62nd Vehicular Technology Conference, 2005.* IEEE, 2005.

[6] Z. B. Tariq, D. M. Cheema, M. Z. Kamran, and I. H. Naqvi, "Non-GPS positioning systems," *ACM Computing Surveys*, vol. 50, no. 4, pp. 1–34, nov 2017.

[7] F. Zafari, A. Gkelias, and K. K. Leung, "A survey of indoor localization systems and technologies," *IEEE Communications Surveys & Tutorials*, vol. 21, no. 3, pp. 2568–2599, 2019.

[8] G. M. Mendoza-Silva, J. Torres-Sospedra, and J. Huerta, "A meta-review of indoor positioning systems," *Sensors*, vol. 19, no. 20, p. 4507, oct 2019.

[9] J. Torres-Solis, T. H., and T. Chau, "A review of indoor localization technologies: towards navigational assistance for topographical disorientation," in *Ambient Intelligence*. InTech, mar 2010.

[10] F. Alkhawaja, M. Jaradat, and L. Romdhane, "Techniques of indoor positioning systems (IPS): A survey," in *2019 Advances in Science and Engineering Technology International Conferences (ASET)*. IEEE, mar 2019.

[11] T. Gigl, G. J. Janssen, V. Dizdarevic, K. Witrisal, and Z. Irahhauten, "Analysis of a uwb indoor positioning system based on received signal strength," in *2007 4th Workshop on Positioning, Navigation and Communication*. IEEE, mar 2007.

[12] J. Kulmer, S. Hinteregger, B. Grosswindhager, M. Rath, M. S. Bakr, E. Leitinger, and K. Witrisal, "Using DecaWave UWB transceivers for high-accuracy multipath-assisted indoor positioning," in *2017 IEEE International Conference on Communications Workshops (ICC Workshops)*. IEEE, may 2017.

[13] A. Alarifi, A. Al-Salman, M. Alsaleh, A. Alnafessah, S. Al-Hadhrami, M. Al-Ammar, and H. Al-Khalifa, "Ultra wideband indoor positioning technologies: Analysis and recent advances," *Sensors*, vol. 16, no. 5, p. 707, may 2016.

[14] Y. Li, Z. Ghassemlooy, X. Tang, B. Lin, and Y. Zhang, "A VLC smartphone camera based indoor positioning system," *IEEE Photonics Technology Letters*, vol. 30, no. 13, pp. 1171–1174, jul 2018.

[15] J. Xu, C. Gong, and Z. Xu, "Experimental indoor visible light positioning systems with centimeter accuracy based on a commercial smartphone camera," *IEEE Photonics Journal*, vol. 10, no. 6, pp. 1–17, dec 2018.

[16] A. Chizari, M. V. Jamali, S. Abdollahramezani, J. A. Salehi, and A. Dargahi, "Visible light for communication, indoor positioning, and dimmable illumination: A system design based on overlapping pulse position modulation," *Optik*, vol. 151, pp. 110–122, dec 2017.

[17] W. Guan, Y. Wu, S. Wen, H. Chen, C. Yang, Y. Chen, and Z. Zhang, "A novel three-dimensional indoor positioning algorithm design based on visible light communication," *Optics Communications*, vol. 392, pp. 282–293, jun 2017.

[18] T.-H. Do, J. Hwang, and M. Yoo, "TDoA based indoor visible light positioning systems," in *2013 Fifth International Conference on Ubiquitous and Future Networks (ICUFN)*. IEEE, jul 2013.

[19] T. Aguilera, F. J. Alvarez, D. Gualda, J. M. Villadangos, A. Hernandez, and J. Urena, "Performance improvement of an ultrasonic LPS by applying a multipath compensation algorithm," in *2017 IEEE International Instrumentation and Measurement Technology Conference (I2MTC)*. IEEE, may 2017.

[20] D. J. Carter, B. J. Silva, U. M. Qureshi, and G. P. Hancke, "An ultrasonic indoor positioning system for harsh environments," in *IECON 2018 - 44th Annual Conference of the IEEE Industrial Electronics Society*. IEEE, oct 2018.

[21] F. Evennou and F. Marx, "Advanced integration of WiFi and inertial navigation systems for indoor mobile positioning," *EURASIP Journal on Advances in Signal Processing*, vol. 2006, no. 1, apr 2006.

[22] G. Retscher, "Test and integration of location sensors for a multi-sensor personal navigator," *Journal of Navigation*, vol. 60, no. 1, pp. 107–117, dec 2006.

[23] L. Zheng, W. Zhou, W. Tang, X. Zheng, A. Peng, and H. Zheng, "A 3d indoor positioning system based on low-cost MEMS sensors," *Simulation Modelling Practice and Theory*, vol. 65, pp. 45–56, jun 2016.

[24] A. Bahillo, I. Angulo, E. Onieva, A. Perallos, and P. Fernandez, "Low-cost bluetooth foot-mounted IMU for pedestrian tracking in industrial environments," in *2015 IEEE International Conference on Industrial Technology (ICIT)*. IEEE, mar 2015.
[25] Z. Kasmi, A. Norrdine, and J. Blankenbach, "Towards a decentralized magnetic indoor positioning system," *Sensors*, vol. 15, no. 12, pp. 30 319–30 339, dec 2015.
[26] B. Gozick, K. P. Subbu, R. Dantu, and T. Maeshiro, "Magnetic maps for indoor navigation," *IEEE Transactions on Instrumentation and Measurement*, vol. 60, no. 12, pp. 3883–3891, dec 2011.
[27] J. Chung, M. Donahoe, C. Schmandt, I.-J. Kim, P. Razavai, and M. Wiseman, "Indoor location sensing using geo-magnetism," in *Proceedings of the 9th international conference on Mobile systems, applications, and services*. ACM Press, 2011.
[28] H. Xie, T. Gu, X. Tao, H. Ye, and J. Lu, "A reliability-augmented particle filter for magnetic fingerprinting based indoor localization on smartphone," *IEEE Transactions on Mobile Computing*, vol. 15, no. 8, pp. 1877–1892, aug 2016.
[29] C. E. Galvan-Tejada, J. P. Garcia-Vazquez, J. I. Galvan-Tejada, and R. Brena, "Multivariate or univariate model analysis for indoor location systems: A comparison," in *2015 International Conference on Electronics, Communications and Computers (CONIELECOMP)*. IEEE, feb 2015.
[30] E. Prigge and J. How, "Signal architecture for a distributed magnetic local positioning system," *IEEE Sensors Journal*, vol. 4, no. 6, pp. 864–873, dec 2004.
[31] J. Blankenbach and A. Norrdine, "Position estimation using artificial generated magnetic fields," in *2010 International Conference on Indoor Positioning and Indoor Navigation*. IEEE, sep 2010.
[32] G. Pirkl and P. Lukowicz, "Robust, low cost indoor positioning using magnetic resonant coupling," in *Proceedings of the 2012 ACM Conference on Ubiquitous Computing - 12*. ACM Press, 2012.
[33] V. Pasku, A. D. Angelis, M. Dionigi, G. D. Angelis, A. Moschitta, and P. Carbone, "A positioning system based on low frequency magnetic fields," *IEEE Transactions on Industrial Electronics*, pp. 1–1, 2015.
[34] A. Sheinker, B. Ginzburg, N. Salomonski, L. Frumkis, B.-Z. Kaplan, and M. B. Moldwin, "A method for indoor navigation based on magnetic beacons using smartphones and tablets," *Measurement*, vol. 81, pp. 197–209, mar 2016.
[35] A. Sheinker, B. Ginzburg, N. Salomonski, and A. Engel, "Localization of a mobile platform equipped with a rotating magnetic dipole source," *IEEE Transactions on Instrumentation and Measurement*, vol. 68, no. 1, pp. 116–128, jan 2019.
[36] T. E. Abrudan, Z. Xiao, A. Markham, and N. Trigoni, "Distortion rejecting magneto-inductive three-dimensional localization (MagLoc)," *IEEE Journal on Selected Areas in Communications*, vol. 33, no. 11, pp. 2404–2417, nov 2015.
[37] A. Plotkin and E. Paperno, "3-d magnetic tracking of a single subminiature coil with a large 2-d array of uniaxial transmitters," *IEEE Transactions on Magnetics*, vol. 39, no. 5, pp. 3295–3297, sep 2003.
[38] N. Derby and S. Olbert, "Cylindrical magnets and ideal solenoids," *American Journal of Physics*, vol. 78, no. 3, pp. 229–235, mar 2010.
[39] F. Masiero. (2020, Sep.) Magnetic field modeling. GitHub. https://github.com/ApeParrot/Magnetic-Field-Modeling.
[40] S. Song, C. Hu, B. Li, X. Li, and M. Q.-H. Meng, "An electromagnetic localization and orientation method based on rotating magnetic dipole," *IEEE Transactions on Magnetics*, vol. 49, no. 3, pp. 1274–1277, mar 2013.
[41] R. Kusche and M. Ryschka, "Combining bioimpedance and EMG measurements for reliable muscle contraction detection," *IEEE Sensors Journal*, vol. 19, no. 23, pp. 11 687–11 696, dec 2019.
[42] R. Kusche, F. John, M. Cimdins, and H. Hellbruck, "Contact-free biosignal acquisition via capacitive and ultrasonic sensors," *IEEE Access*, vol. 8, pp. 95 629–95 641, 2020.
[43] O. Kypris, T. E. Abrudan, and A. Markham, "Magnetic induction-based positioning in distorted environments," *IEEE Transactions on Geoscience and Remote Sensing*, vol. 54, no. 8, pp. 4605–4612, aug 2016.